Simulated Connections between ENSO and Tropical Cyclones near Guam in a High-Resolution GFDL Coupled Climate Model: Implications for Seasonal Forecasting

WEI ZHANG

National Oceanic and Atmospheric Administration/Geophysical Fluid Dynamics Laboratory, and Atmospheric and Oceanic Sciences Program, Princeton University, Princeton, New Jersey, and IIHR—Hydroscience and Engineering, The University of Iowa, Iowa City, Iowa, and Key Laboratory of Meteorological Disaster, Ministry of Education, and Collaborative Innovation Center on Forecast and Evaluation of Meteorological Disasters, Nanjing University of Information Science and Technology, Nanjing, China

GABRIEL A. VECCHI

National Oceanic and Atmospheric Administration/Geophysical Fluid Dynamics Laboratory, and Atmospheric and Oceanic Sciences Program, Princeton University, Princeton, New Jersey

GABRIELE VILLARINI

IIHR—Hydroscience and Engineering, The University of Iowa, Iowa City, Iowa

HIROYUKI MURAKAMI, THOMAS DELWORTH, AND LIWEI JIA

National Oceanic and Atmospheric Administration/Geophysical Fluid Dynamics Laboratory, and Atmospheric and Oceanic Sciences Program, Princeton University, Princeton, New Jersey

RICHARD GUDGEL AND FANRONG ZENG

National Oceanic and Atmospheric Administration/Geophysical Fluid Dynamics Laboratory, Princeton, New Jersey

(Manuscript received 9 February 2016, in final form 17 August 2016)

ABSTRACT

This study aims to assess the connections between El Niño–Southern Oscillation (ENSO) and tropical cyclones near Guam (GuamTCs) using the state-of-the-art Geophysical Fluid Dynamics Laboratory (GFDL) Forecast-Oriented Low Ocean Resolution version of CM2.5 (FLOR). In observations, more (fewer) GuamTCs occur in El Niño (La Niña) years, and the ENSO–GuamTC connections arise from TC genesis locations in ENSO phases. The observed ENSO–GuamTC connections are realistically simulated in the two control experiments that use two versions of FLOR: the standard version and another with flux adjustments (FLOR-FA). The ENSO–GuamTC connections in FLOR-FA are closer to observations than those in FLOR because of a better representation of TC genesis during ENSO phases. The physical mechanisms underlying the observed ENSO–GuamTC connections are further supported in the long-term control experiments with FLOR and FLOR-FA. The ENSO–GuamTC connections in sea surface temperature (SST)- and sea surface salinity (SSS)-restoring experiments with FLOR 1990 strongly resemble the observations, suggesting the ENSO–GuamTC connections arise substantially from the forcing of SST. The prediction skill of FLOR-FA for GuamTC frequency is quite promising in terms of correlation and root-mean-square error and is higher than that of FLOR for the period 1980–2014. This study shows the capability of global climate models (FLOR and FLOR-FA) in simulating the linkage between ENSO and TC activity near a highly localized region (i.e., Guam) and in predicting the frequency of TCs at the subbasin scale.

Supplemental information related to this paper is available at the Journals Online website: http://dx.doi.org/10.1175/JCLI-D-16-0126.s1.

Corresponding author address: Wei Zhang, Ph.D., National Oceanic and Atmospheric Administration/Geophysical Fluid Dynamics Laboratory, 201 Forrestal Rd., Princeton, NJ 08540.
E-mail: wei.zhang@noaa.gov

DOI: 10.1175/JCLI-D-16-0126.1

1. Introduction

Tropical cyclones (TCs) exert tremendous damage to coastal and inland regions by causing torrential rainfall, strong winds, landslides, floods, and debris flows (e.g., Pielke and Landsea 1999; Rappaport 2000; Pielke et al. 2008; Zhang et al. 2009). It is therefore of scientific and societal value to better understand the variability and predictability of TCs.

Among some of the major drivers of TC variability on seasonal-to-interannual time scales, El Niño–Southern Oscillation (ENSO) plays a major role. ENSO is a strong atmosphere–ocean coupled climate phenomenon in the tropical Pacific (e.g., Philander 1983; Rasmusson and Wallace 1983; Zebiak and Cane 1987), and it influences weather and climate not only in the tropical Pacific but also in midlatitude and even polar regions (e.g., Ropelewski and Halpert 1986; Gloersen 1995; Zhang and Held 1999; Lau and Nath 2000; Straus and Shukla 2002). ENSO strongly modulates the frequency, genesis, and tracks of TCs in the North Atlantic (e.g., Goldenberg and Shapiro 1996; Bove et al. 1998; Pielke and Landsea 1999), western North Pacific (WNP; e.g., Chan 1985; Wang and Chan 2002; Camargo and Sobel 2005; Zhang et al. 2012, 2015, 2016b), and South Pacific (Revell and Goulter 1986; Basher and Zheng 1995). In addition to the impacts of ENSO on TCs in ocean basins, previous studies have also found the modulation of ENSO on TCs influencing special regions such as the Hawaiian Islands (Chu and Wang 1997, 1998; Clark and Chu 2002), Fiji (Chand and Walsh 2009, 2011), and the Caribbean (Gianniniet al. 2001; Tartaglione et al. 2003). Guam, which is in the western Pacific Ocean, is frequently impacted by TCs, with consequences for TC-related disaster risk and water resource management as TCs account for around 30% of the total annual rainfall (Rodgers et al. 2000; Kubota and Wang 2009). Guam is also a U.S. military installation close to Asia, which makes TC forecasts for Guam a matter of national security. A recent study reported that TCs in the Pacific islands are more frequent yet much less studied than those in the North Atlantic (Marler 2014). Few studies have been devoted to the analysis of TCs affecting Guam (GuamTCs). Lander (1994) found a larger number of GuamTCs during El Niño years than La Niña years. Nonetheless, the physical mechanisms underlying such a relationship are yet to be disentangled.

Climate models have been widely used to investigate the ENSO–TC connections (e.g., Vitart and Stockdale 2001; Wu and Lau 1992; Bell et al. 2014; Zhang et al. 2016b). A new high-resolution coupled climate model has been developed at the National Oceanic and Atmospheric Administration (NOAA)/Geophysical Fluid Dynamics Laboratory (GFDL), called the GFDL Forecast-Oriented Low Ocean Resolution version of CM2.5 (FLOR; e.g., Vecchi et al. 2014; Jia et al. 2015; Yang et al. 2015). FLOR is used to produce real-time seasonal forecasts as part of the North American Multimodel Ensemble (NMME; Kirtman et al. 2014). It has been used to examine regional seasonal TC activity and has successfully simulated and predicted regional climate over many regions of the world (Vecchi et al. 2014; Jia et al. 2015; Yang et al. 2015; Zhang et al. 2016a,b,c,d). FLOR has been used to analyze the responses of TCs to ENSO and anthropogenic radiative forcing across tropical basins (Vecchi et al. 2014; Murakami et al. 2015a,b; Krishnamurthy et al. 2016; Zhang et al. 2016b). It is thus of great interest to assess the performance of FLOR in simulating ENSO–GuamTC connections in FLOR and to examine the robustness of such connections in the long control experiments with FLOR.

In summary, this study aims at disentangling the physical mechanisms underpinning the ENSO–GuamTC connections, evaluating the robustness of the connections in FLOR control experiments, assessing the performance of FLOR in reproducing these connections, and examining the capability of FLOR in seasonal forecasting of the occurrence frequency of GuamTC.

The remainder of this study is organized as follows. Section 2 presents data and methodology, followed by section 3 where we present the results of our analyses using the GFDL FLOR climate model. Finally, section 4 summarizes the main points of the study and concludes the paper.

2. Data and methodology

a. Data

The TC data are obtained from the International Best Track Archive for Climate Stewardship (IBTrACS; Knapp et al. 2010).The key meteorological variables (e.g., wind fields) are obtained from the Japan Meteorological Agency (JMA) Japanese 55-year Reanalysis (JRA-55) data (Kobayashi et al. 2015). To substantiate the results, the National Centers for Environmental Prediction (NCEP)–National Center for Atmospheric Research (NCAR) reanalysis (Kalnay et al. 1996) data are also used. The JRA-55 is available since 1958 on a global basis with a spatial resolution of 1.25° × 1.25°. It is based on a new data assimilation system that reduces many of the problems reported in the first JMA reanalysis (Kobayashi et al. 2015). Monthly estimates of sea surface temperature (SST) are taken from the Met Office Hadley Centre SST dataset (HadSST3.1.1.0; Kennedy et al. 2011). Niño-3 and Niño-3.4 indices are

defined as the SST anomalies averaged over the regions 5°S–5°N, 90°–150°W and 5°S–5°N, 170°E–120°W, respectively. The SST anomalies in observations are defined on the base period 1971–2000, while those in the FLOR and flux-adjusted version of FLOR (FLOR-FA) simulations are based on the simulated climatology of FLOR and FLOR-FA. The El Niño and La Niña years are defined based on the Niño-3.4 index, which represents the SST anomalies averaged over the region 5°S–5°N, 170°E–120°W. The July–October (JASO) months during which the Niño-3.4 index is larger (smaller) than one standard deviation are designated as El Niño (La Niña). The central Pacific (CP) El Niño is not considered because there are few CP El Niño events in the control experiments of FLOR and FLOR-FA. The relative lack of CP El Niño events in these simulations may be linked to their excessive weakening of the trade winds in the eastern equatorial Pacific during El Niño. This overly weakens the equatorial upwelling in that region, biasing the anomalous SST warming toward the eastern rather than central Pacific.

b. TCs near Guam

GuamTCs are defined as TCs for which the tracks intersect a 500-km buffer zone around Guam during their life-span in the peak season (JASO). The results are similar if we change the definition of peak season from JASO to either June–November (JJASON) or June–October (JJASO). TCs are defined as those storms with intensity level of tropical storm or above. The selection of 500 km as the size of the buffer zone is similar to the definition of Hawaii TCs (Murakami et al. 2013). Moreover, the results are similar if we change the buffer zone size of GuamTCs from 300 to 700 km.

c. Global coupled model

The experiments in this study are performed with GFDL FLOR, which is characterized by high-resolution land and atmosphere components and a relatively low-resolution ocean component (Vecchi et al. 2014). The atmosphere and land components of FLOR are taken from GFDL CM2.5 with a spatial resolution of 50 km × 50 km (Delworth et al. 2012), while its ocean and sea ice components (with 1° × 1° spatial resolution) are similar to those in the CM2.1 (Delworth et al. 2006). This study also utilizes FLOR-FA (Vecchi et al. 2014). More details about the FLOR and FLOR-FA models are documented in Vecchi et al. (2014), Jia et al. (2015), Yang et al. (2015), and references therein.

d. Control simulation

We use two long control experiments with FLOR and FLOR-FA. A 500-yr control simulation that incorporates radiative forcing and land use representative of 1990 with FLOR-FA (FLOR-FA 1990; ''present-day experiment'') is analyzed to characterize the ENSO–GuamTC connections. We also analyze a similar control experiment that does not incorporate flux adjustments and FLOR 1990 (1000 yr). The two control experiments enable the analysis of the robustness of the ENSO–GuamTC connections to the role flux adjustments play in such connections.

e. SST-nudging experiments

In addition to the control experiments with FLOR 1990, we use the restoring–nudging experiments in which sea surface salinity (SSS) and SST are restored–nudged to observational estimates of climatological SSS and interannually varying monthly SST at time scales of 5 and 10 days. The simulated SSS and SST are restored to the *World Ocean Atlas 2005* (Antonov et al. 2006) and the Hadley Centre Sea Ice and SST dataset (HadISST1.1; Rayner et al. 2003), respectively. Because both restoring experiments at time scales of 5 and 10 days have the same prescribed SST and SSS, these experiments enable the diagnosis of whether and to what extent the simulated ENSO–GuamTC association arises from the performance of the SST simulation. More details about restoring–nudging experiments can be found in Murakami et al. (2015b) and Zhang et al. (2016b).

f. Seasonal forecasting experiments

The GFDL's Ensemble Coupled Data Assimilation (ECDA) system is used to initialize the seasonal forecasting experiments with FLOR (Zhang et al. 2007; Zhang and Rosati 2010; Chang et al. 2013). The ECDA is updated in every month for the seasonal-to-decadal forecasting experiments of GFDL (Yang et al. 2013, 2015; Vecchi et al. 2013, 2014; Msadek et al. 2014; Jia et al. 2015). More details of FLOR's seasonal forecasting experiments are provided in Vecchi et al. (2014).

3. Analysis results

a. Observations and control experiments

The simulated TC density climatology with FLOR and FLOR-FA is compared with that in the observations. The spatial pattern of TC density simulated by FLOR 1990 is shifted eastward compared to the observations (Fig. 1). In contrast, the pattern of TC density climatology simulated with FLOR-FA 1990 is more realistic than those in FLOR 1990 (Fig. 1). In general, the two control experiments produce a higher TC density than observations in the WNP including the region near

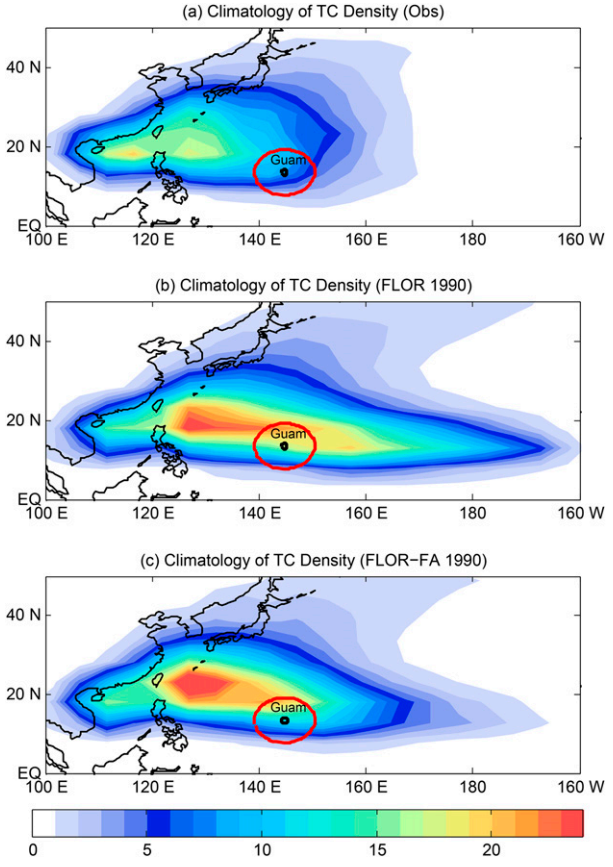

FIG. 1. Climatology of TC density in JASO in the WNP [color shading; occurrences (TCseason)$^{-1}$] in (a) observations (GuamTC = 5.8), (b) FLOR 1990 (GuamTC = 10.7), and (c) FLOR-FA 1990 (GuamTC = 9.1). The thick black polygon and the red outer circle denote Guam and its 500-km buffer zone, which is used to define GuamTC. TCseason is defined as JASO.

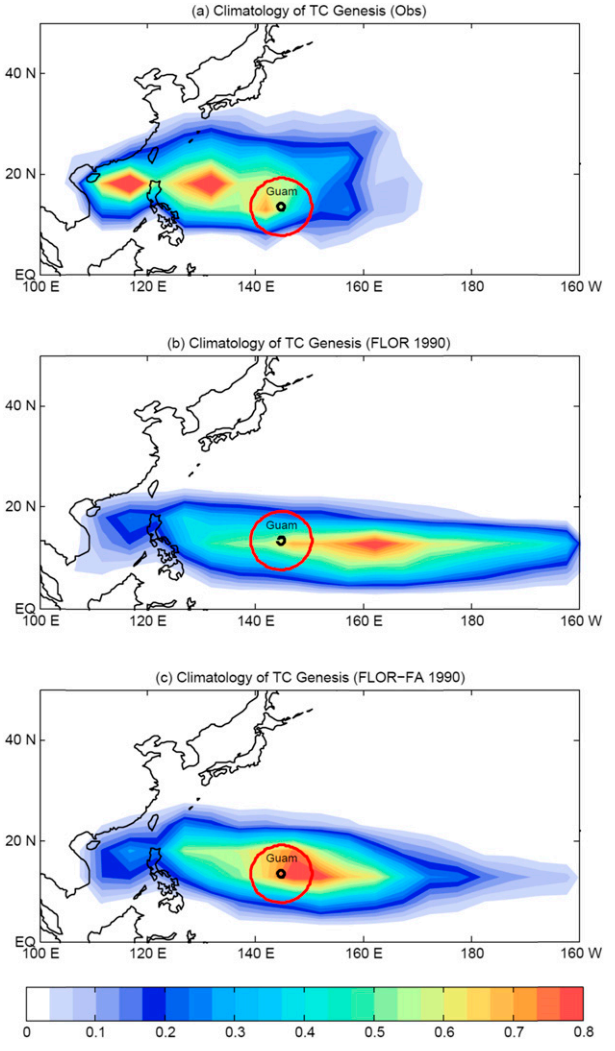

FIG. 2. As in Fig. 1, but for TC genesis in the peak season.

Guam (Fig. 1). The climatology of TC density near Guam in the control experiments is higher than that in observations (Fig. 1). Similarly, the TC genesis climatology simulated in FLOR-FA is more realistic than FLOR (Fig. 2) as FLOR exhibits a more pronounced eastward bias, as with TC density. The TC-genesis density near Guam with FLOR-FA 1990 is higher than that in the observations, while FLOR 1990 produces TC genesis near Guam similar to observations (Fig. 2). Figure 3 illustrates the climatology of SST, 850-hPa relative vorticity, 600-hPa relative humidity, and vertical wind shear (VWS; 200–850 hPa), which are closely related to TC genesis in observations, FLOR 1990, and FLOR-FA 1990 control experiments. FLOR 1990 and FLOR-FA 1990 capture the climatology of these key variables in the western Pacific reasonably well (Fig. 3). The mean SST in FLOR 1990 and FLOR-FA 1990 is shifted eastward to the central Pacific compared with that in the observations (Figs. 3a–c). The 850-hPa relative vorticity climatology patterns in the observations as well as the FLOR and FLOR-FA 1990 control experiments are similar to one another (Figs. 3d–f). The 850-hPa relative humidity in the FLOR and FLOR-FA 1990 control experiments is stronger than that in the observations, especially in the central Pacific where TC geneses in FLOR and FLOR-FA occurs (Figs. 3g–i). The VWS climatology in FLOR and FLOR-FA bears strong resemblance to that in the observations with slightly weaker VWS in the southeastern WNP and the central Pacific (Figs. 3j–l). Therefore, FLOR and FLOR-FA realistically simulate the climatology of key variables related to TC genesis. The biases in the key variables with FLOR and FLOR-FA are consistent with the eastward shift of TC genesis in FLOR and FLOR-FA compared with observations.

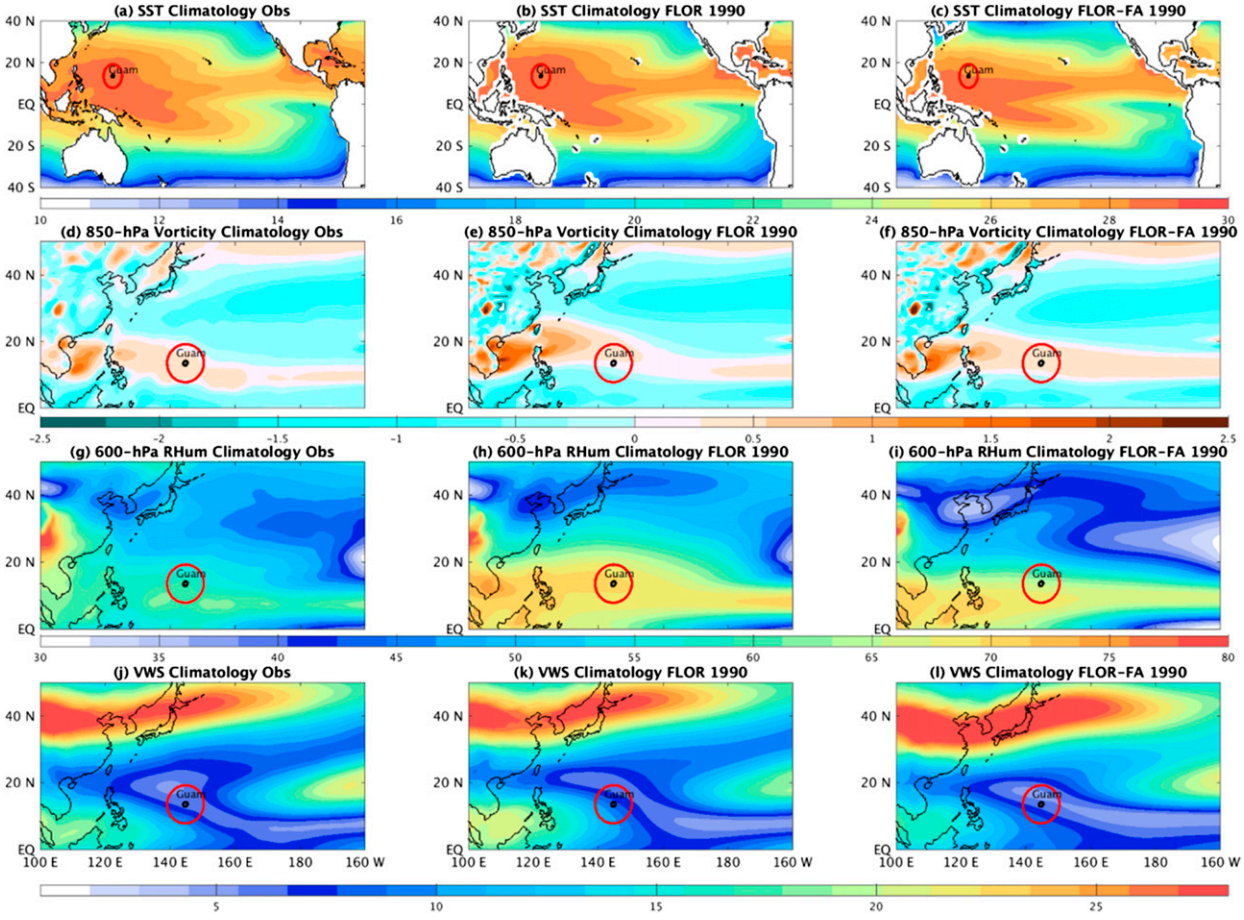

FIG. 3. Climatology of (a)–(c) SST (°C) in JASO, (d)–(f) 850-hPa relative vorticity (10^{-5} s^{-1}), (g)–(i) 600-hPa relative humidity (%), and (j)–(l) VWS (m s^{-1}) in (left)–(right) observations, FLOR 1990, and FLOR-FA 1990 control experiments. The inner black symbol and the red outer circle denote Guam and its 500-km buffer zone.

The correlation coefficients between GuamTC and Niño indices (Niño-3 and Niño-3.4) in the observations are positive and significant at the 0.01 level during the 1965–2014 period (Table 1), suggesting an increased (decreased) number of GuamTCs during El Niño (La Niña) years. We also show the correlation between GuamTC and Niño indices in the long-term control experiments of FLOR and FLOR-FA. Table 1 shows that all the correlation coefficients between GuamTC and Niño indices in all the control experiments are statistically significant at the 0.01 level and generally comparable with those from the observations. However, there are some differences in the values of the correlation coefficients among different control experiments (Table 1). For example, Niño-3 and Niño-3.4 have a higher correlation with GuamTC in FLOR-FA 1990 than in FLOR 1990 (Table 1). The difference in the correlation coefficients between FLOR-FA 1990 and FLOR 1990 is significant at the 0.01 level based on a z test (Table 1). Although the simulation length for FLOR-FA 1990 is 500 yr, while that for FLOR 1990 is 1000 yr, the correlations in each 500-yr subperiod of FLOR 1990 are nearly the same as those over the entire 1000-yr period. Therefore, the correlation coefficients between Niño indices and the occurrence of GuamTCs are greater in FLOR-FA than those in FLOR experiments, and the difference is significant between FLOR and FLOR-FA 1990 control experiments. Moreover, the simulated ENSO–GuamTC connections in the control experiments of FLOR and

TABLE 1. The correlation coefficients between GuamTCs and El Niño indices (Niño-3 and Niño-3.4) in observations and in the control experiments of GFDL FLOR 1990 and FLOR-FA 1990. All the correlation coefficients are significant at the 0.01 level.

GuamTC and ENSO	Niño-3	Niño-3.4
Observations (1965–2014)	0.48	0.55
FLOR 1990 (1000 yr)	0.21	0.29
FLOR-FA 1990 (500 yr)	0.54	0.54

FLOR-FA are consistent with the observations, indicating that the observed ENSO–GuamTC association is robust and can be well reproduced by the GFDL FLOR coupled climate model.

To disentangle the physical mechanisms underlying the ENSO–GuamTC connections, we examine the regression of JASO TC density, genesis, and steering flow (here defined as 500-hPa wind fields) in the WNP onto the concurrent Niño-3.4 index in the observations and the FLOR and FLOR-FA control experiments (Fig. 4). In the observations, positive regressions of TC density are observed in the vicinity of Guam with respect to the Niño-3.4 index, suggesting a higher (lower) GuamTC density during El Niño (La Niña) years. Similar spatial regression patterns of TC density around Guam are found for the FLOR and FLOR-FA control experiments. In other words, the TC density around Guam is higher during El Niño years than during La Niña years in both observations and FLOR and FLOR-FA control experiments (Fig. 4). This study uses the Student's t test for the significance analysis of the regression coefficient β and the t score is calculated as $\beta/\mathrm{std}(\beta)$, with the standard deviation given as "std." Therefore, some locations with small regression coefficient β are statistically significant owing to the small standard deviation of β there (Fig. 4). This applies to the following discussions of the hypothesis test for the regression coefficients of TC genesis and density onto Niño indices. It is noted that the regions of positive TC density regressions in FLOR 1990 simulations are shifted eastward to the central Pacific compared with the observations (Fig. 4). The eastward shift in TC density with respect to observations in FLOR-FA, however, is less marked than that in FLOR, indicating that FLOR-FA outperforms FLOR in simulating TC density in the WNP from this perspective. This shift in the regression of TC density (Fig. 4) is closely associated with that in the climatology of TC density in simulations with FLOR and FLOR-FA (Fig. 1) owing to their similarity. The eastward shift in TC density of FLOR and FLOR-FA has also been identified in Vecchi et al. (2014) and Krishnamurthy et al. (2016). Moreover, the shift in TC density is mainly influenced by TC genesis and track, both strongly determined by the steering flow, which is analyzed to further diagnose the ENSO–GuamTC (density) association discussed above.

The regression of TC genesis onto the Niño-3.4 index in observations and FLOR and FLOR–FA control experiments is shown in Fig. 5. Both observations and control experiments with FLOR show a southeast–northwest pattern of TC genesis in the WNP (Fig. 5), which has been widely discussed in previous studies

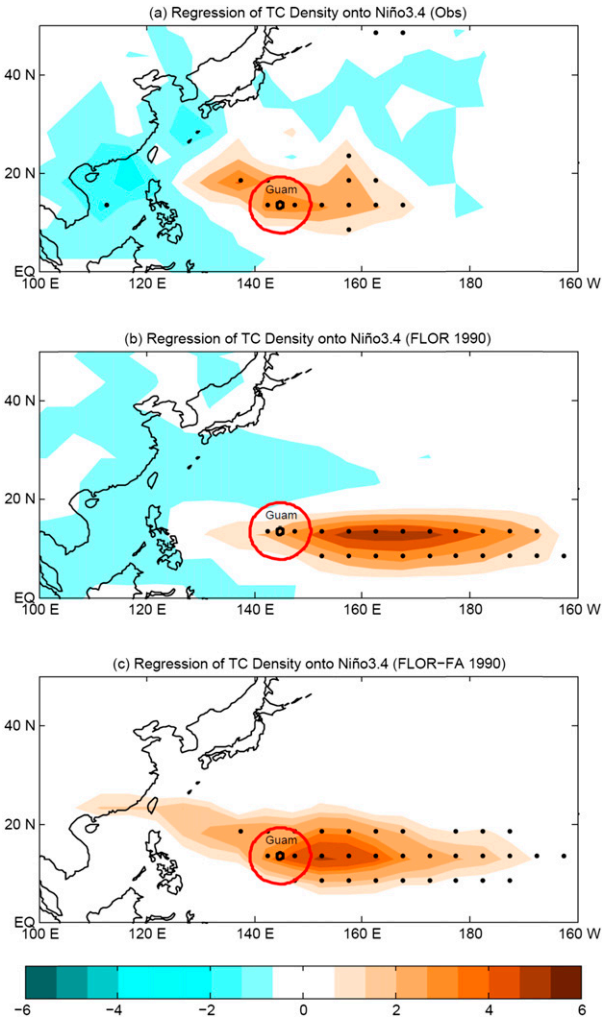

FIG. 4. Regression of TC density in the peak season (JASO) in the WNP [color shading; occurrences (TCseason^{-1}) °C^{-1}] onto the Niño-3.4 index in (a) observations, (b) FLOR 1990, and (c) FLOR-FA 1990 control experiments. The black-dot-stippled regions represent regression coefficients that are statistically significant at the 0.05 level. The black thick marker and the red outer circle denote Guam and its 500-km buffer zone.

(e.g., Wang and Chan 2002; Camargo et al. 2007; Zhang et al. 2016b). Similar to the regression of TC density onto Niño-3.4, the regression of TC genesis in the WNP in FLOR and FLOR-FA is also shifted eastward toward the central Pacific, and the shift in FLOR-FA is less marked than that in FLOR (Fig. 5). This eastward shift (Fig. 5) is also associated with that in the climatology of TC genesis (Fig. 2). The regression of TC genesis in the vicinity of Guam (inside the red circle) in the observations is very different from those in FLOR and FLOR-FA (Fig. 5). Specifically, the regression in the observations is positive while it is largely negative in FLOR and negative (positive) in the northwestern (southeastern)

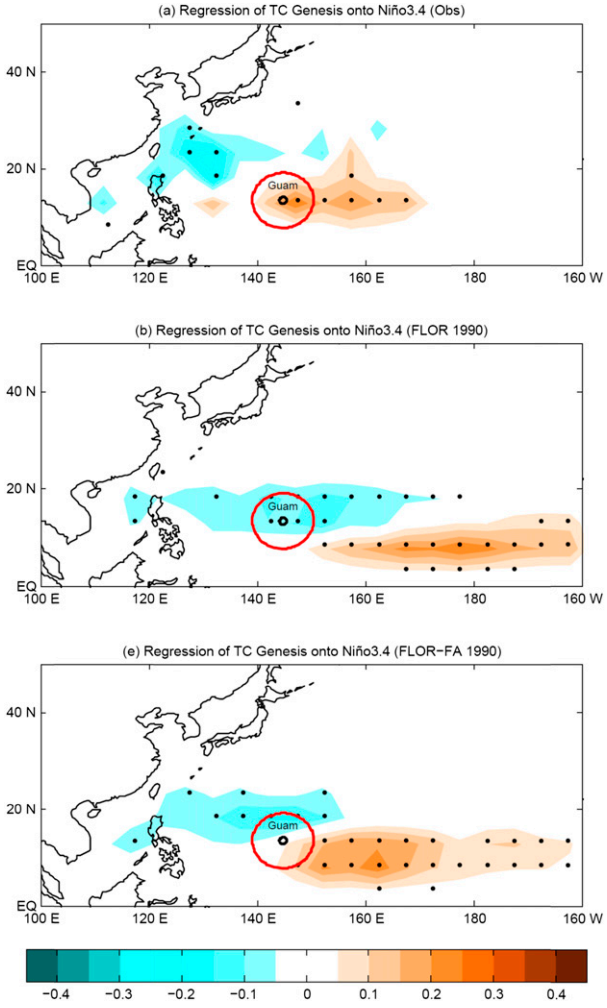

FIG. 5. As in Fig. 4, but for TC genesis.

part in FLOR-FA (Fig. 5). This suggests that, while both FLOR and FLOR-FA are different from the observations, FLOR-FA outperforms FLOR in simulating the linkage between TC genesis near Guam and ENSO. The regression of TC genesis near Guam onto the Niño-3.4 index in FLOR-FA is still shifted eastward to the observations.

To further diagnose the physical mechanisms underlying changes in TC genesis during El Niño–La Niña years, we analyze the genesis potential index (GPI; Emanuel and Nolan 2004) in observations and models. The GPI climatology in FLOR and FLOR-FA control experiments is higher than that in the observations (Fig. 6). The FLOR and FLOR-FA control experiments produce higher GPI in the southeastern WNP and in the central Pacific than the observations (Figs. 6a–c), consistent with the eastward shift in TC genesis in FLOR and FLOR-FA (Fig. 5). During El Niño–La Niña years, there is a southeast–northwest pattern in GPI in observations and models, similar to that in regression of TC genesis onto Niño-3.4 (Fig. 6). The southeast–northwest pattern in WNP TC genesis during El Niño–La Niña years has been widely reported in previous studies (Wang and Chan 2002; Camargo et al. 2007). Therefore, the GPI climatology and anomalies during El Niño–La Niña years are largely consistent with those in TC genesis in the observations, FLOR, and FLOR-FA.

Figure 7 shows SST, 850-hPa relative vorticity, 600-hPa relative humidity, and VWS anomalies during El Niño years in the observations and FLOR 1990 and FLOR-FA 1990 control experiments. FLOR and FLOR-FA capture fundamental characteristics of these key variables in the observations during El Niño years (Fig. 7). The spatial patterns of key variables related to TC genesis in the observations and FLOR and FLOR-FA control experiments are consistent with those of GPI in El Niño years (Figs. 6 and 7). For example, the anomalies of 850-hPa relative vorticity and VWS in FLOR-FA are stronger than those in FLOR in the southeastern WNP during El Niño years, consistent with a higher GPI anomaly in FLOR-FA during El Niño years (Figs. 6 and 7). The FLOR 1990 and FLOR-FA 1990 control experiments capture the observed fundamental characters of these key variables in La Niña years (Fig. 8). FLOR-FA simulate slightly more realistic anomalies of key variables than FLOR during La Niña years (Fig. 8). Note that the VWS anomalies in FLOR-FA are stronger than those in FLOR during La Niña years, with FLOR-FA closer to the observations (Fig. 8). Therefore, FLOR and FLOR-FA simulate realistic TC genesis climatology and anomalies during El Niño–La Niña years, though both models produce an eastward shift in TC genesis. This shift is associated with a similar shift in GPI and the anomalies in related key variables (e.g., 850-hPa relative vorticity and VWS). Figure 9 shows the regression of steering flow onto the Niño-3.4 index and TC density differences between El Niño and La Niña years in observations and FLOR and FLOR-FA simulations. The regression of steering flow to the Niño-3.4 index is quite weak in the Guam domain, compared with the climatology of steering flow (Figs. 9 and 10). The climatology of steering flow is mainly easterly flow, which is conducive to GuamTCs (Fig. 10). However, the strongest signal of steering flow in the observations and FLOR and FLOR-FA control experiments during Niño is the anomalous westerly located south of Guam and closer to the equator where few TCs are formed (Fig. 9). In addition, the other less strong signal of steering flow is the anomalous southerly flow to the north of Guam

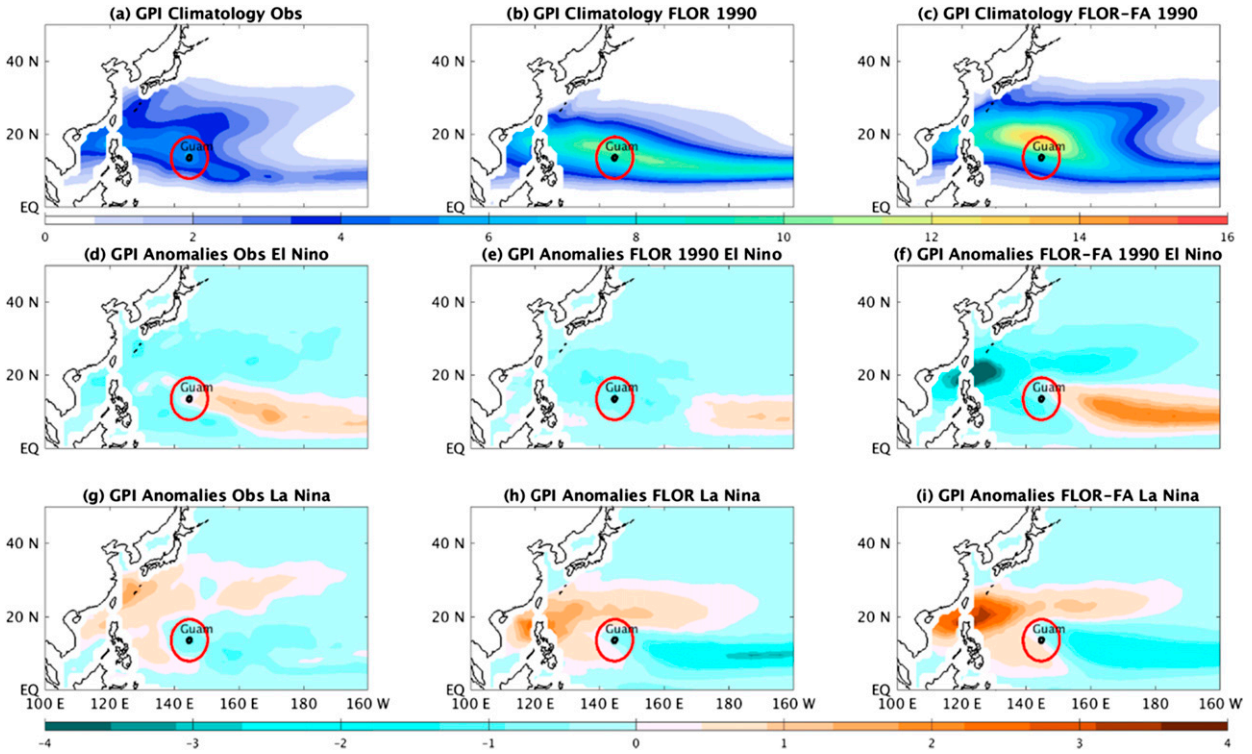

FIG. 6. The GPI (a)–(c) climatology and anomalies during (d)–(f) El Niño and (g)–(i) La Niña years in the (left)–(right) observations, FLOR, and FLOR-FA 1990 control experiments. The inner black symbol and the red outer circle denote Guam and its 500-km buffer zone.

(Figs. 9). Therefore, the strong steering flow anomalies in the two regions lead to minor changes in GuamTC. Furthermore, the steering flow is characterized by weak or zero westerlies when averaged over Guam's vicinity (Fig. 9). The influences of ENSO on GuamTCs, therefore, arise mainly from the changes in TC genesis locations instead of steering flow in both observations and FLOR and FLOR-FA control experiments. During El Niño (La Niña) years, there are more (less) TC geneses east of or near Guam. WNP TCs mostly move northwestward by beta effect and climatological easterly steering flow after they are formed. Therefore, TCs tend to move toward Guam if TC geneses are shifted eastward during El Niño years. During La Niña years, there are fewer GuamTCs because TCs are suppressed east of Guam compared with El Niño years. Therefore, FLOR and FLOR-FA realistically simulate the ENSO–GuamTC connections shown in the observations, and the physical mechanisms underlying the connections in the observations are similar to those in FLOR and FLOR-FA.

The control experiments of FLOR and FLOR-FA discussed above are fully coupled simulations (free run). SST-nudging experiments enable further diagnosis of the contribution of SST forcing to the ENSO–GuamTC connections and their results are presented next.

b. *Results from SST-nudging experiments with FLOR 1990*

The six-member SST- and SSS-nudging experiments with FLOR 1990 for the period 1971–2012 are utilized to further diagnose the contribution of SST to the ENSO–GuamTC connections. Figure 11 shows the climatology of TC density in observations and FLOR 1990 SST-nudging experiments for 1971–2012. In general, FLOR 1990 generates higher TC density than the observations in the WNP, especially east of the Philippines. TC density climatology in the vicinity of Guam in FLOR 1990 SST-nudging experiments is also higher than that in the observations, similar to the relationship between observed and simulated TC density in control experiments with FLOR and FLOR-FA (Fig. 11). The locations with the largest values of TC genesis in FLOR 1990 are different from those in the observations. Specifically, the observed locations with the largest values of TC genesis climatology are located in the South China Sea and the Philippine Sea, while those in FLOR 1990 SST-nudging experiments are shifted eastward to 140°–160°E (Fig. 12). The TC

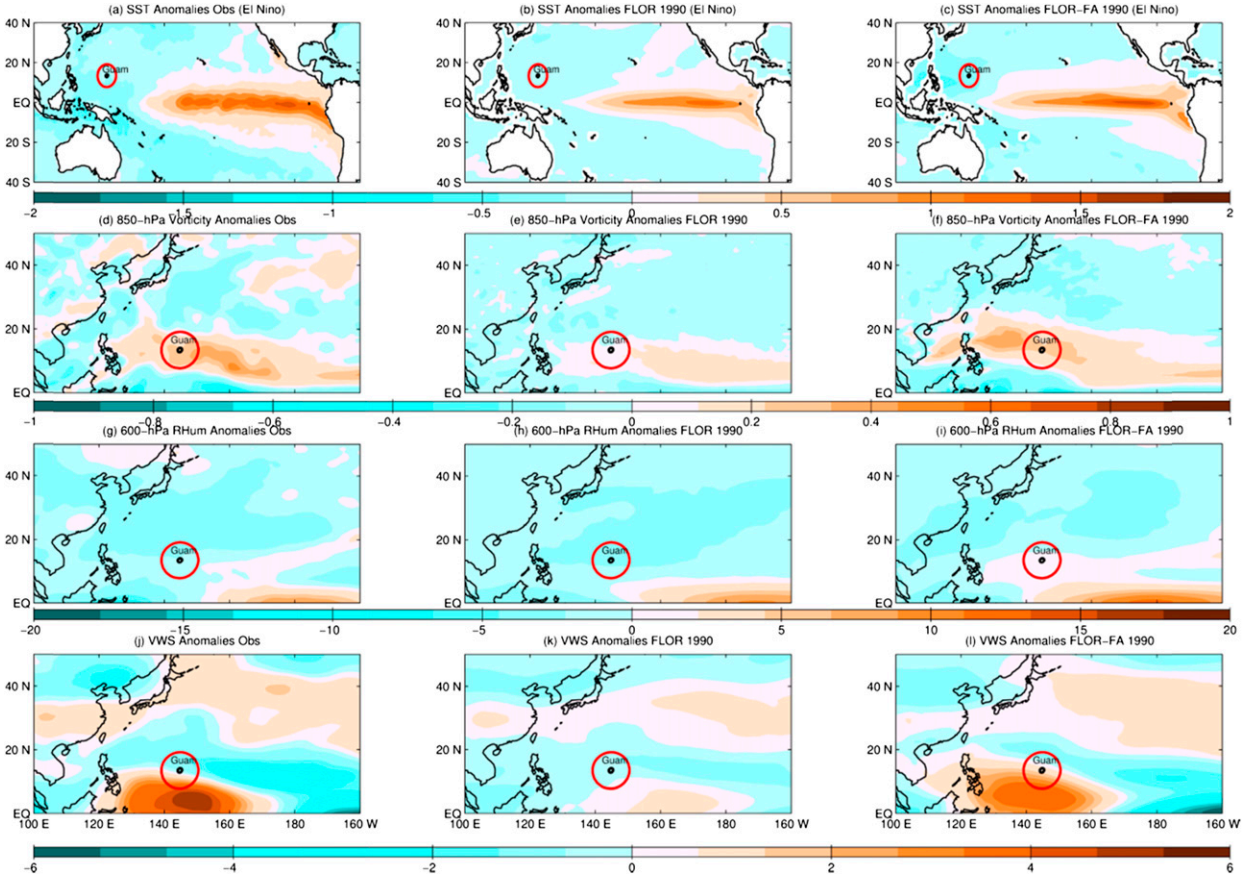

FIG. 7. The (a)–(c) SST (°C), (d)–(f) 850-hPa relative vorticity (10^{-5} s^{-1}), (g)–(i) 600-hPa relative humidity (%), and (j)–(l) vertical wind shear (m s^{-1}) anomalies during El Niño years in the (left)–(right) observations, FLOR, and FLOR-FA 1990 control experiments. The inner black symbol and the red outer circle denote Guam and its 500-km buffer zone.

genesis climatology in the vicinity of Guam in FLOR 1990 SST-nudging experiments is higher than that in the observations (Fig. 12).

The correlations between Niño indices and GuamTCs for the period 1971–2012 are significant at the 0.01 level and are similar to those in FLOR 1990 SST-nudging experiments, though the values of correlation based on the observations are slightly larger than those in the SST-nudging experiments (Table 2). Therefore, the forcing of SST plays a dominant role in the ENSO–GuamTC connections. Moreover, the correlations between Niño indices and GuamTCs in FLOR 1990 SST-nudging experiments are significantly higher than those in the FLOR 1990 control experiment based on a z test, further supporting the important role of SST forcing in the ENSO–GuamTC connections.

The regression of TC density onto the Niño-3.4 index for 1971–2012 in the observations resembles that of FLOR 1990 SST-nudging experiments, with positive regression coefficients in the Guam domain (Fig. 13). There is also an eastward shift in TC density in FLOR 1990 SST-nudging experiments compared to the observations, similar to those in the control experiments (Fig. 13). Such a shift in the regions of positive regressions (Fig. 13) is associated with the shift in the simulated climatology of TC density (Fig. 11). The regression of TC genesis onto the Niño-3.4 index in FLOR 1990 SST-nudging experiments is also similar to that in the observations, except that there is an eastward shift in the spatial pattern of SST-nudging experiments (Fig. 14). However, the spatial patterns of TC genesis in the Guam domain between observations and the FLOR 1990 SST-nudging experiments are different. The regressions of TC genesis around Guam are positive in the observations, whereas they are mostly negative in FLOR 1990 SST-nudging experiments (Fig. 14).

The climatology of GPI in the observations and FLOR 1990 SST-nudging experiments has a similar pattern with a higher magnitude in FLOR 1990 SST-nudging experiments, especially in the southeastern WNP and the central Pacific, consistent with the eastward shift in

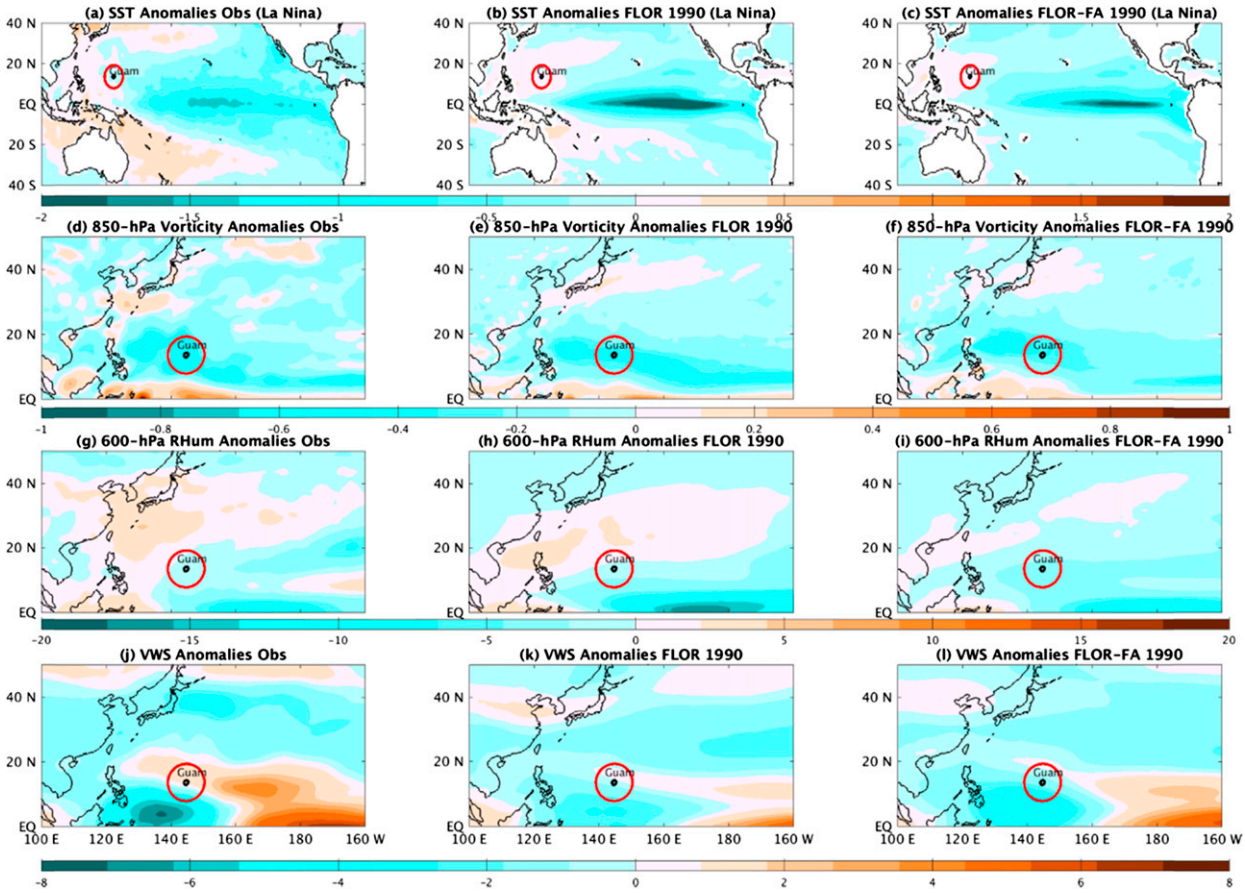

FIG. 8. As in Fig. 7, but for La Niña years.

TC genesis climatology (Figs. 15a,b). The spatial patterns of GPI anomalies in FLOR 1990 SST-nudging experiments are similar to those in the observations during El Niño–La Niña years, with stronger anomalies in FLOR 1990 SST-nudging experiments (Figs. 15c–f).

The steering flow regressed onto Niño-3.4 in the observations is quite similar to that in the SST-nudging experiments with FLOR, especially in the Guam domain (Fig. 16). The anomalous steering flow during Niño is quite weak in the Guam domain, compared with the climatology of steering flow (Fig. 16 and Fig. S1 in the supplementary information). The climatology of steering flow in the SST-nudging experiments with FLOR is mainly easterly, which is conducive to GuamTCs (see Fig. S1). Similar to the discussions on steering flow in the observations and FLOR and FLOR-FA control experiments in section 3a, the regions with a strong signal of steering flow are located in regions with few TC geneses (i.e., south and north of Guam; Fig. 16). Therefore, the impacts of ENSO on GuamTCs are largely caused by TC genesis locations other than steering flow in the SST-nudging experiments with FLOR. Although the regressions for TC genesis in FLOR SST-nudging experiments are shifted eastward in contrast to the observations (Fig. 14), TC density regressions around Guam in the observations resemble those in the experiments (Fig. 16). Therefore, GuamTCs come mainly from TCs east of Guam that move westward or northwestward during El Niño years. Based on the above discussions, SST plays a dominant role in the ENSO–GuamTC connections because of its modulation on TC genesis patterns.

The free run with FLOR 1990 shows differences with the SST-nudging experiment of FLOR 1990 in the responses of GuamTC-genesis density to ENSO. Not surprisingly, the flux-adjustment version of FLOR 1990 produces the responses of GuamTC-genesis density to ENSO very similar to the SST-nudging experiment with FLOR 1990. For example, the responses of steering flow (Figs. 9 and 16), GuamTC genesis (Figs. 5 and 13), and GuamTC density (Figs. 4 and 13) to ENSO in FLOR-FA 1990 are closer to the observations than FLOR.

This study suggests that FLOR performs well in capturing TC frequency near Guam, despite the fact that TC geneses in FLOR and FLOR-FA are shifted eastward.

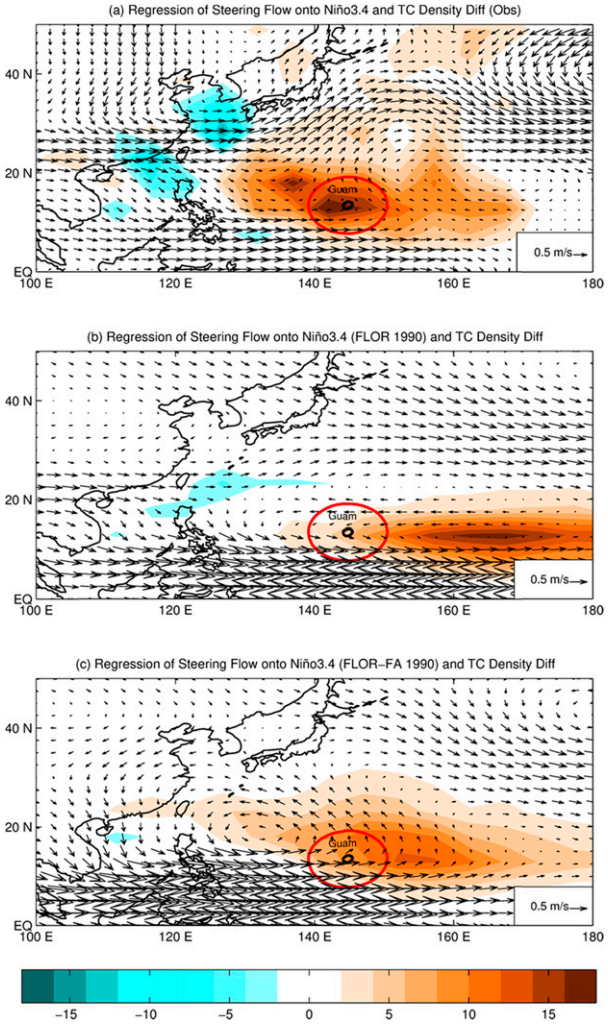

FIG. 9. Regression of steering flow (vectors, $m\,s^{-1}\,°C^{-1}$, see legend at bottom right of each panel) onto Niño-3.4 index and TC density difference (color shading, El Niño minus La Niña) in (a) observations, (b) FLOR 1990, and (c) FLOR-FA 1990 control experiments. The black circle and the red outer circle denote Guam and its 500-km buffer zone.

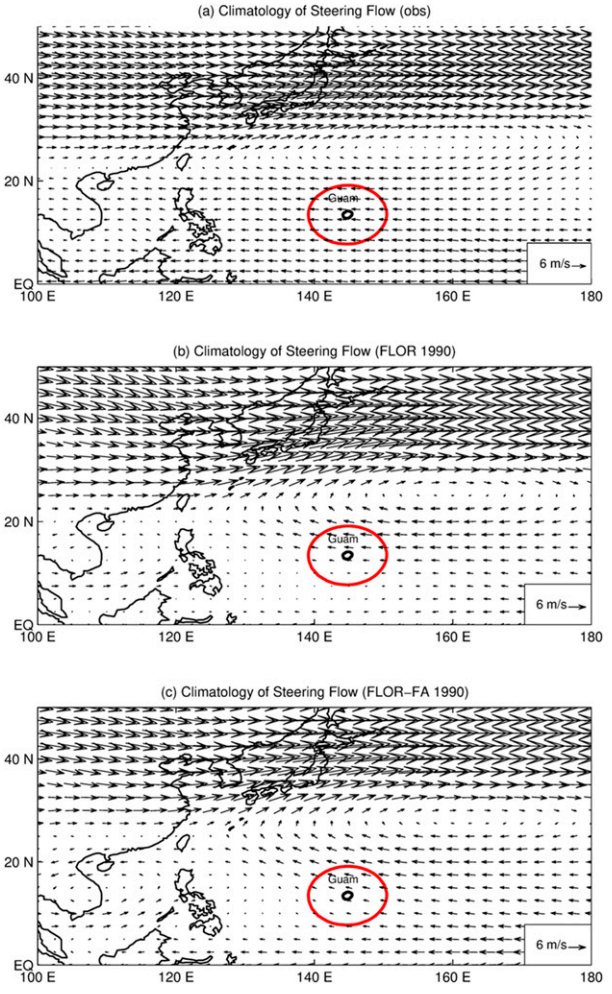

FIG. 10. Climatology of steering flow (vectors, $m\,s^{-1}$, see legend at bottom right of each panel) in (a) observations, (b) FLOR 1990, and (c) FLOR-FA 1990 control experiments. The black circle and the red outer circle denote Guam and its 500-km buffer zone.

During El Niño (La Niña) years, there are more (fewer) TC geneses east of or near Guam in the model. TCs in the WNP mostly move northwestward by beta effect and climatological steering flow. Therefore, TCs tend to move toward Guam if TC geneses are shifted eastward in the model during El Niño years. During La Niña years, there are fewer GuamTCs because TCs are suppressed east of Guam compared with El Niño years.

c. Seasonal forecasting of GuamTCs with FLOR-FA

The findings presented so far have shown that FLOR and FLOR-FA can reproduce the ENSO–GuamTC connections and that SST plays a key role in such connections. Here we analyze the seasonal forecasting of GuamTCs with FLOR-FA for the period of 1980–2014. We analyze the seasonal forecasting experiments in this period initialized in July with 12 ensemble members.

The predicted TC density climatology with FLOR-FA bears strong similarity to that in the observations, especially within the Guam domain (Fig. 17). The TC density centers in FLOR-FA and observations are located east of Taiwan in the Philippine Sea, though the center has a higher density in FLOR-FA (Fig. 17). The predicted TC density climatology in FLOR-FA is shifted eastward compared to the observations (Fig. 17), similar to that in control and SST-nudging experiments. The predicted TC genesis climatology with FLOR-FA is also similar to the observations (Fig. 18). However, it is noted that the predicted TC genesis climatology with

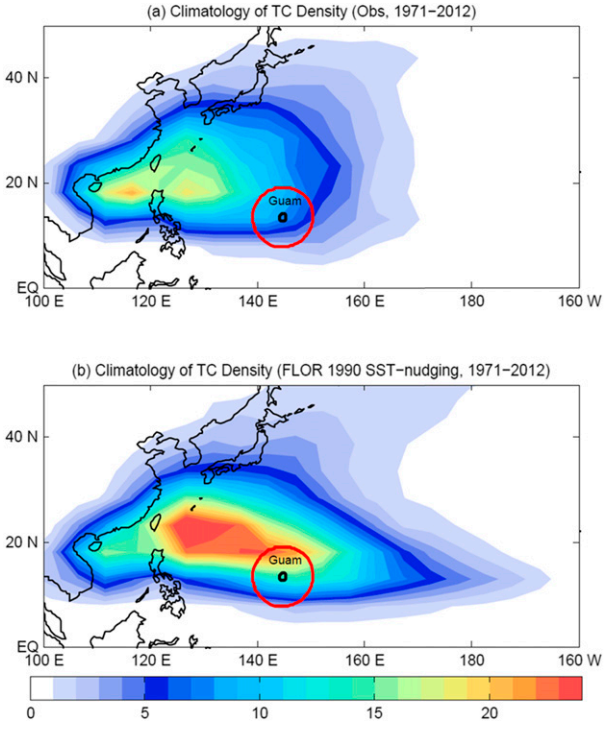

FIG. 11. Climatology of TC density [color shading, occurrences $(\text{TCseason})^{-1}$] in the peak season (JASO) in the WNP in (a) observations (GuamTC = 5.3) and (b) FLOR 1990 SST-nudging experiments (GuamTC = 7.2) for 1971–2012. The black circle and the red outer circle denote Guam and its 500-km buffer zone.

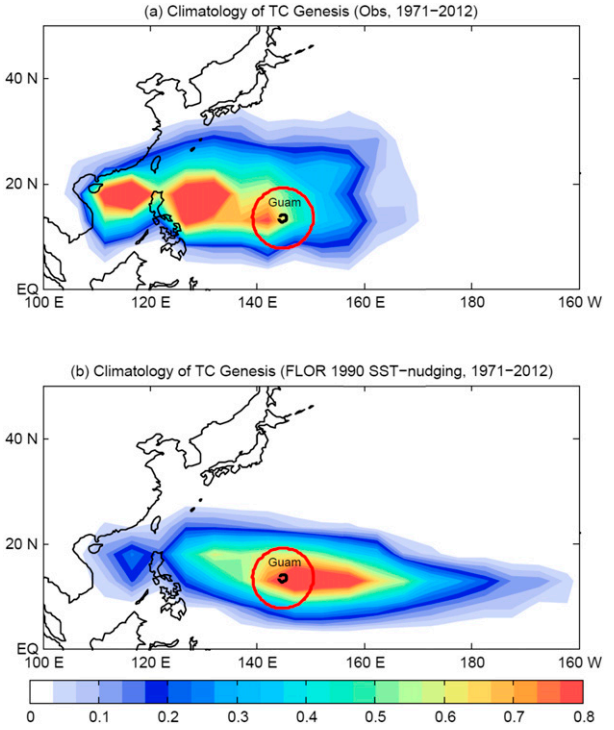

FIG. 12. As in Fig. 11, but for TC-genesis density.

FLOR-FA has one main center while that in the observations consists of three centers. The observed TC genesis climatology center in Guam is well predicted in FLOR-FA (Fig. 18). For further diagnosis, we calculated the spatial correlation map for the predicted and observed TC density in the WNP (Fig. 19). The correlation map is calculated on a 5° × 5° grid in which the correlation between predicted and observed TC counts are for the period 1980–2014. In most of the WNP, there are positive correlation coefficients and the greatest correlation is located in 5°–15°N, 150°–170°E. Within the Guam domain, the correlation is promising, suggesting that FLOR-FA performs well in predicting GuamTCs (Fig. 19). The results here are consistent with Vecchi et al. (2014) in which the correlation between observed and predicted TC density for forecasts initialized in July is high in the vicinity of Guam. Vecchi et al. (2014) used several versions of FLOR to make prediction for TC density, while this study only uses seasonal predictions with FLOR-FA.

The seasonal forecasting of the frequency of GuamTCs initialized in July using FLOR-FA is also promising, with a correlation of 0.57 and a root-mean-square error (RMSE) of 1.92 for the period 1980–2014 (Fig. 20), consistent with the spatial correlation map shown in Fig. 19.

FLOR-FA shows high prediction skill for GuamTCs, and this may arise from the adjusted SST in FLOR-FA in which the climatological adjustments are applied to FLOR-FA's momentum, enthalpy, and freshwater flux from the atmosphere to the ocean to bring the model's SST and surface wind stress climatology closer to the observations (Vecchi et al. 2014). This is supported by considering the differences in predictions between FLOR (i.e., no flux adjustments are applied) and FLOR-FA. The correlation between predicted GuamTC frequency with FLOR and the observations is 0.47 while the RMSE is 2.33 (Fig. 20). Therefore, the prediction skill for the frequency of GuamTCs is higher in FLOR-FA than FLOR in terms of both correlation and RMSE (Fig. 20), confirming the important role of both flux

TABLE 2. The correlation coefficients between GuamTCs and El Niño indices (Niño-3 and Niño-3.4) in observations and in FLOR 1990 SST-nudging experiments with six members for the period 1971–2012. All the correlation coefficients are statistically significant at the 0.01 level.

GuamTC and ENSO	Niño-3	Niño-3.4
Observations (1971–2012)	0.44	0.51
FLOR 1990 (1971–2012, six member)	0.41	0.45

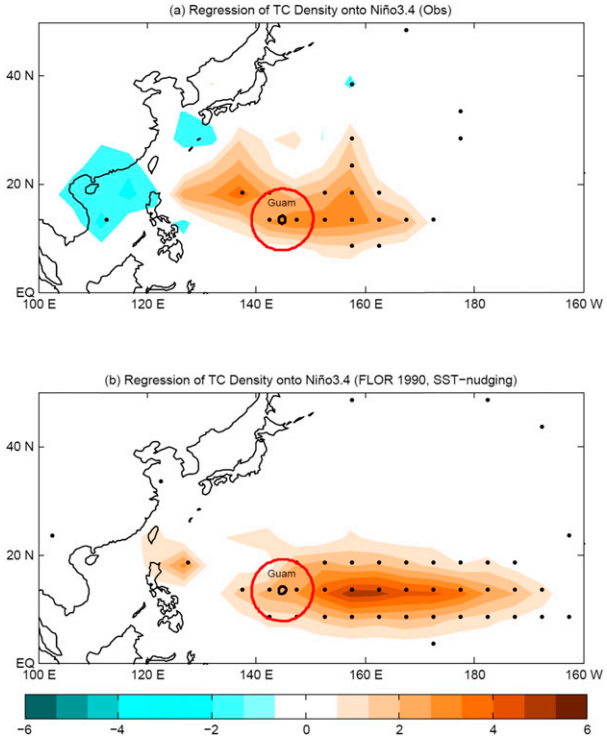

FIG. 13. Regression of TC density in the peak season (JASO) in the WNP [color shading, occurrences (TCseason)$^{-1}$ °C^{-1}] onto the Niño-3.4 index in (a) observations and (b) SST-nudging experiment with FLOR 1990. The black-dot-stippled regions represent regression coefficients that are statistically significant at the 0.05 level. The black circle and the red outer circle denote Guam and its 500-km buffer zone.

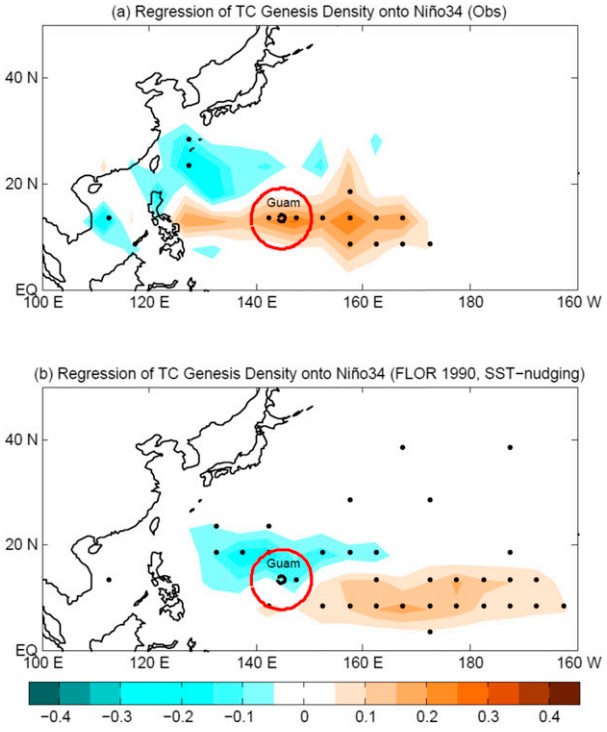

FIG. 14. As in Fig. 13, but TC genesis.

adjustments and SST in skillfully simulating and predicting GuamTCs.

4. Discussion and conclusions

ENSO has a significant association with the frequency of TCs near Guam. This study has examined the physical mechanisms underlying ENSO–GuamTC connections, the robustness of these connections, the performance of FLOR and FLOR-FA in reproducing them in the control experiments, and its prediction skill for GuamTCs. To the best of our knowledge, this is the first study devoted to the ENSO–GuamTC connections.

In the observations, the ENSO–GuamTC connections arise from significant relationships with TC genesis and are statistically significant in the four control experiments (FLOR 1990 and FLOR-FA 1990). The ENSO–GuamTC connections in FLOR-FA are generally closer to observations than those in FLOR because of a better representation of TC genesis in FLOR-FA. The physical mechanisms underlying the observed ENSO–GuamTC connections have been confirmed in the long control experiments with FLOR and FLOR-FA. Using SST-nudging experiments, we have found that the ENSO–GuamTC connections arise substantially from the forcing of SST because the associations between ENSO and GuamTCs are similar in the observations and SST-nudging experiments. The prediction skill (measured in terms of correlation and RMSE) of FLOR with flux adjustments (FLOR-FA) in GuamTC frequency is quite promising and is higher than that in FLOR, confirming the importance of a correct SST climatology for forecasting TCs near Guam.

The physical mechanisms underlying the influences of El Niño and La Niña on WNP TC activity have been thoroughly discussed in Wang and Chan (2002). Figure 21 illustrates the schematic diagram for the physical mechanisms underlying the impacts of El Niño on GuamTCs, and those in La Niña are generally opposite to those in this figure. Figure 21 illustrates that El Niño is associated with surface westerlies in the tropical western and central Pacific. The westerly anomalies are related to strong 850-hPa relative vorticity in the southeastern WNP, leading to more TC geneses (Fig. 21). The cyclonic flow west of the El Niño is forced by classic Matsuno–Gill responses (Matsuno 1966; Gill 1980). The El Niño–induced central Pacific heating also generates a pair of strong anomalous anticyclones in the

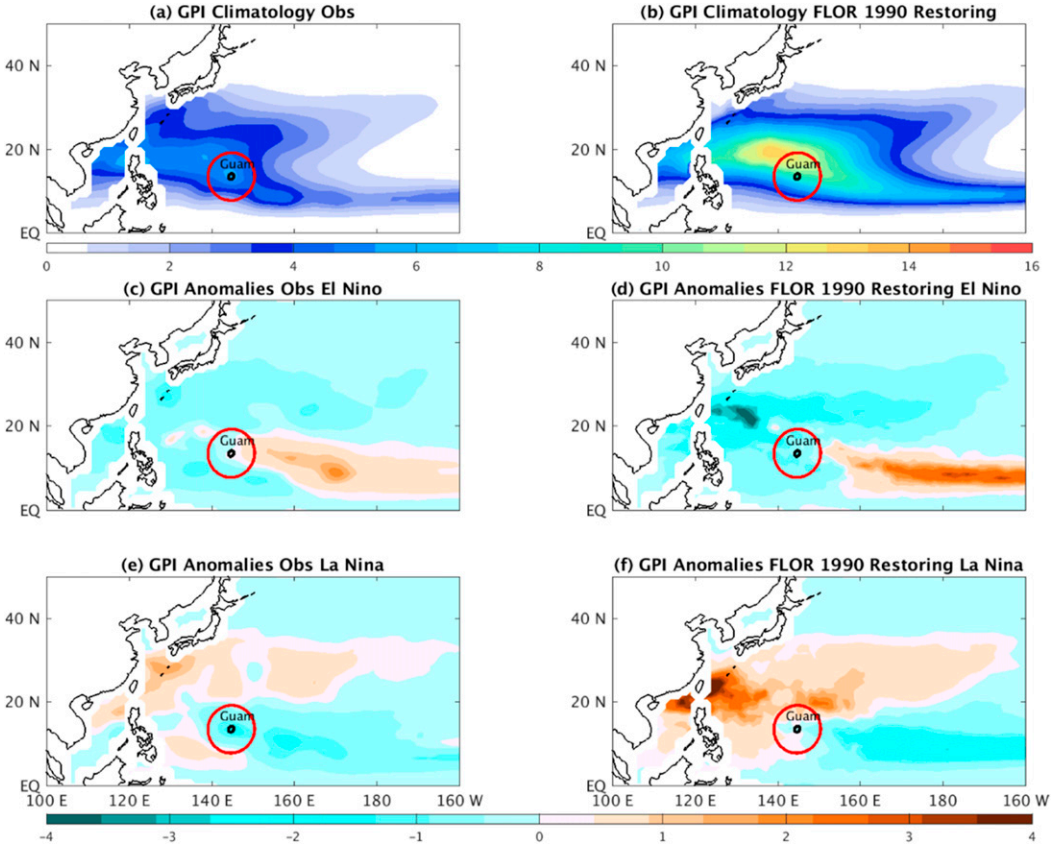

FIG. 15. The GPI (a),(b) climatology (1971–2012) and anomalies during (c),(d) El Niño and (e),(f) La Niña years in the (left) observations and (right) SST-restoring experiment with FLOR 1990. The inner black symbol and the red outer circle denote Guam and its 500-km buffer zone.

upper levels that resides on both sides of the equator, leading to a deepening of the upper-level troughs at 500 and 200 hPa, which strongly suppresses TC genesis in the northwestern part of the WNP and provides a favorable steering flow condition for TC recurvature around 135°E (Fig. 21; Wang and Chan 2002; Wang and Zhang 2002). Such mechanisms are responsible for the southeast–northwest pattern of TC genesis during El Niño–La Niña years. The influences of ENSO on GuamTCs arise mainly from the changes in TC genesis locations instead of steering flow in both observations and FLOR control and SST-nudging experiments.

This study has identified the capability of a global climate model (FLOR and FLOR-FA) in simulating and predicting TC activity near a special region, Guam. This capability arises mainly from the SST forcing and ENSO, which are well represented in FLOR-FA. During El Niño (La Niña) years, there are more (fewer) TC geneses east of or near Guam in the model. TCs in the WNP mostly move northwestward by beta effect and climatological easterly steering flow. Therefore, TCs tend to move toward (away from) Guam in the model and observations during El Niño (La Niña) years. This study confirms the dominant role of ENSO on TC activity near Guam, which is vulnerable to tremendous TC-induced damage. This study encourages us to further understand the connections between ENSO and TC activity in other basins, which may help improve the prediction skill of dynamic, statistical, and hybrid prediction schemes.

Conventional ENSO has no significant association with the peak season basinwide TC frequency in the WNP (e.g., Wang and Chan 2002; Camargo and Sobel 2005). Instead, ENSO leads to a southeast–northwest spatial pattern of WNP TC genesis (Wang and Chan 2002; Camargo and Sobel 2005). In other words, more (less) frequent TC genesis occurs in the southeastern (northwestern) portion of the WNP during El Niño (La Niña) years (Wang and Chan 2002; Camargo et al. 2007). Guam is mainly located in the southeastern (SE) portion of the WNP. This study has shown high predictability of GuamTCs owing largely to the ENSO–GuamTC connections, suggesting that it may be easier to predict TC genesis in the subregions (e.g., SE)

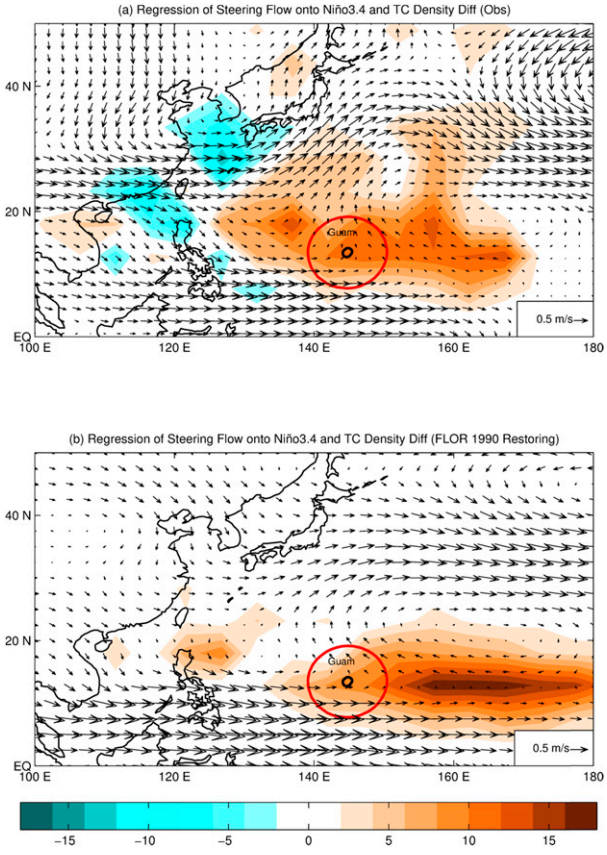

FIG. 16. Regression of steering flow (vectors, m s^{-1} °C^{-1}, see legend at bottom right of each panel) onto the Niño-3.4 index and TC density difference (color shading, El Niño minus La Niña) in the (a) observations and (b) SST-nudging experiments with FLOR 1990. The black circle and the outer red circle denote Guam and its 500-km buffer zone.

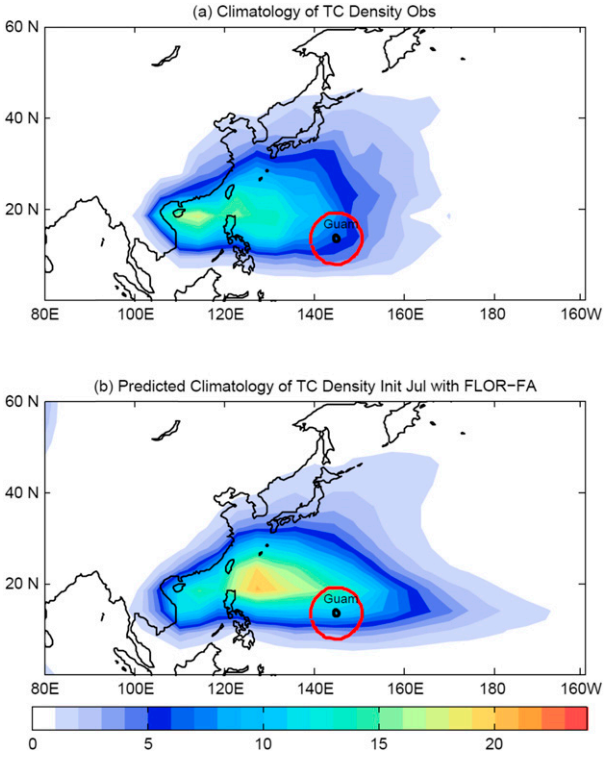

FIG. 17. The (a) observed (GuamTC = 5.1) and (b) predicted (FLOR-FA, GuamTC = 5.7) TC density climatology in the peak season (JASO) in the WNP [color shading, occurrences $(\text{TCseason})^{-1}$]. The black symbol and the red outer circle denote Guam and its 500-km buffer zone.

of the WNP. This hypothesis will be tested in our future work using both observations and FLOR and FLOR-FA simulations.

Acknowledgments. The authors are grateful to the editor and two anonymous reviewers for their insightful comments. The authors acknowledge Carlos Gaitan and Nat Johnson for their helpful comments on an earlier version of this manuscript. This material is based in part upon work supported by the National Science Foundation under Grants AGS-1262091 and AGS-1262099.

APPENDIX

Tracking Algorithm

The TCs in FLOR and FLOR-FA are tracked from 6-hourly model output by using the tracker developed at GFDL and implemented in Murakami et al. (2015a,b) and Zhang et al. (2016a,b). The temperature anomaly t_a averaged vertically over 300 and 500 hPa, 10-m wind speed, 850-hPa relative vorticity, and sea level pressure (SLP) are key components of this tracker. The tracking procedures are as follows.

1) Local minima are found for the smoothed SLP field. The location of the cyclone center is properly adjusted by fitting a biquadratic surface to the SLP and locating the center at the minima.
2) Closed contours are generated in an interval dp of 2 hPa around every single low center. The Nth contour is marked as the contiguous region surrounding a low central pressure P with pressures lower than dp × N + P, as detected by a "flood fill" algorithm. The contours are not required to be circular, and a maximum radius of 3000 km is searched from each candidate SLP low center.
3) If the above closed contours are found, the low is counted as a potential TC center. In this way, the tracker attempts to find all closed contours within a certain distance of the low center and without entering contours belonging to another low. The maximum

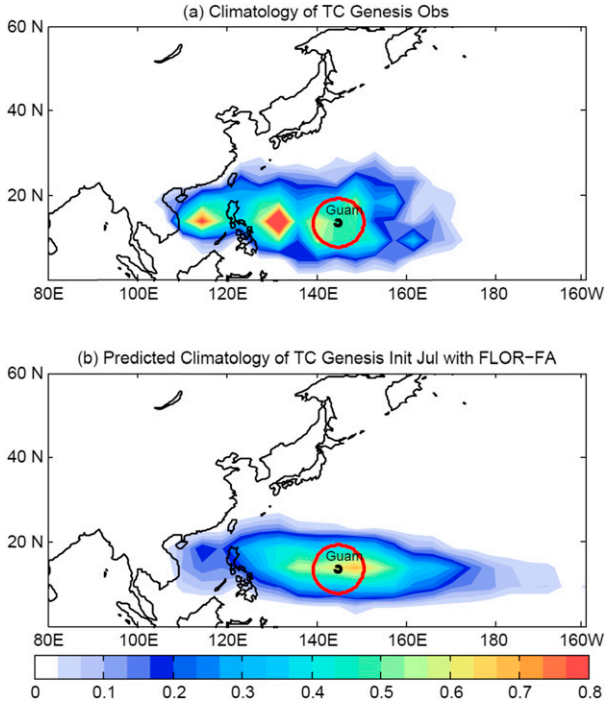

FIG. 18. The (a) observed and (b) predicted (FLOR-FA; initialized in July) TC genesis climatology in the peak season (JASO) for 1980–2014 in the WNP [color shading, occurrences $(\text{TCseason})^{-1}$]. The black symbol and the red outer circle denote Guam and its 500-km buffer zone.

10-m wind inside the set of closed contours is taken as the maximum wind speed at that time for the storm.

4) To test if the potential TC center meets the requirement of a warm core, we follow a similar process. Closed 1-K contours are found surrounding the maximum t_a within a TC's identified contours, at no more than 1° from the location of the center of the low. The contour with the largest value must be within 1° of the center of the low and must have a radius smaller than 3°; otherwise the low is not considered warm core and the center is rejected.
5) TC centers are combined into a TC track by connecting the low centers at 6-h intervals. A deeper low center has higher priority of tracking.
6) The following criteria are required to finalize the TC identifications:

(i) at least 72 h of total detection lifetime (not necessarily consecutive),
(ii) at least 48 cumulative (not necessarily consecutive) hours with a warm core,
(iii) at least 36 consecutive hours of a warm core with winds $>17.5\,\text{m s}^{-1}$, and

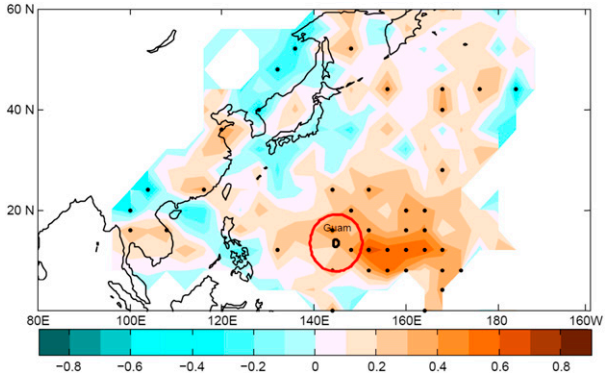

FIG. 19. Spatial correlation map between predicted (FLOR-FA, initialized in July) and observed TC density in 1980–2014 in the WNP. The black-dot-stippled regions represent regression coefficients that are statistically significant at the 0.05 level. The black polygon symbol and the red outer circle denote Guam and its 500-km buffer zone.

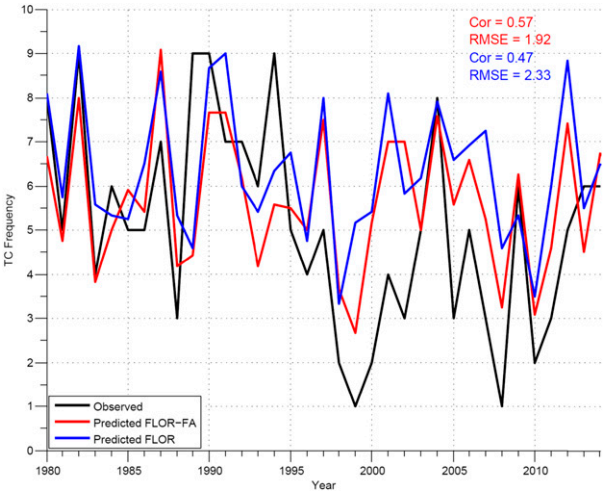

FIG. 20. The predicted frequency of JASO GuamTCs with FLOR-FA (red) and FLOR (blue) initialized in July and the observations (black) for the period of 1980–2014. Correlation coefficient (Cor) and root-mean-square error (RMSE) are also given.

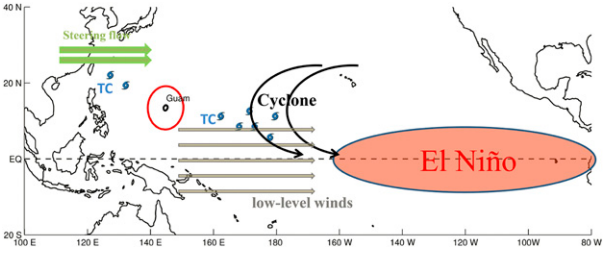

FIG. 21. Schematic diagram on how El Niño influences GuamTC. The impacts of La Niña on GuamTCs are in general opposite to the mechanisms in this figure. The black symbol and the red outer circle denote Guam and its 500-km buffer zone.

(iv) TC genesis confined equatorward of 40°N.

TC track–genesis density in the WNP is binned into 5° × 5° grid boxes at a 6-h interval without smoothing.

REFERENCES

Antonov, J. I., R. A. Locarnini, T. P. Boyer, A. V. Mishonov, and H. E. Garcia, 2006: *Salinity*. Vol. 2, *World Ocean Atlas 2005*, NOAA Atlas NESDIS 62, 182 pp.

Basher, R., and X. Zheng, 1995: Tropical cyclones in the southwest Pacific: Spatial patterns and relationships to Southern Oscillation and sea surface temperature. *J. Climate*, **8**, 1249–1260, doi:10.1175/1520-0442(1995)008<1249:TCITSP>2.0.CO;2.

Bell, R., K. Hodges, P. L. Vidale, J. Strachan, and M. Roberts, 2014: Simulation of the global ENSO–tropical cyclone teleconnection by a high-resolution coupled general circulation model. *J. Climate*, **27**, 6404–6422, doi:10.1175/JCLI-D-13-00559.1.

Bove, M. C., J. J. O'Brien, J. B. Eisner, C. W. Landsea, and X. Niu, 1998: Effect of El Niño on U.S. landfalling hurricanes, revisited. *Bull. Amer. Meteor. Soc.*, **79**, 2477–2482, doi:10.1175/1520-0477(1998)079<2477:EOENOO>2.0.CO;2.

Camargo, S. J., and A. H. Sobel, 2005: Western North Pacific tropical cyclone intensity and ENSO. *J. Climate*, **18**, 2996–3006, doi:10.1175/JCLI3457.1.

——, K. A. Emanuel, and A. H. Sobel, 2007: Use of a genesis potential index to diagnose ENSO effects on tropical cyclone genesis. *J. Climate*, **20**, 4819–4834, doi:10.1175/JCLI4282.1.

Chan, J. C. L., 1985: Tropical cyclone activity in the northwest Pacific in relation to the El Niño/Southern Oscillation phenomenon. *Mon. Wea. Rev.*, **113**, 599–606, doi:10.1175/1520-0493(1985)113<0599:TCAITN>2.0.CO;2.

Chand, S. S., and K. J. E. Walsh, 2009: Tropical cyclone activity in the Fiji region: Spatial patterns and relationship to large-scale circulation. *J. Climate*, **22**, 3877–3893, doi:10.1175/2009JCLI2880.1.

——, and ——, 2011: Influence of ENSO on tropical cyclone intensity in the Fiji region. *J. Climate*, **24**, 4096–4108, doi:10.1175/2011JCLI4178.1.

Chang, Y.-S., S. Zhang, A. Rosati, T. Delworth, and W. Stern, 2013: An assessment of oceanic variability for 1960–2010 from the GFDL ensemble coupled data assimilation. *Climate Dyn.*, **40**, 775–803, doi:10.1007/s00382-012-1412-2.

Chu, P.-S., and J. Wang, 1997: Tropical cyclone occurrences in the vicinity of Hawaii: Are the differences between El Niño and non–El Niño years significant? *J. Climate*, **10**, 2683–2689, doi:10.1175/1520-0442(1997)010<2683:TCOITV>2.0.CO;2.

——, and ——, 1998: Modeling return periods of tropical cyclone intensities in the vicinity of Hawaii. *J. Appl. Meteor.*, **37**, 951–960, doi:10.1175/1520-0450(1998)037<0951:MRPOTC>2.0.CO;2.

Clark, J. D., and P.-S. Chu, 2002: Interannual variation of tropical cyclone activity over the central North Pacific. *J. Meteor. Soc. Japan*, **80**, 403–418, doi:10.2151/jmsj.80.403.

Delworth, T. L., and Coauthors, 2006: GFDL's CM2 global coupled climate models. Part I: Formulation and simulation characteristics. *J. Climate*, **19**, 643–674, doi:10.1175/JCLI3629.1.

——, and Coauthors, 2012: Simulated climate and climate change in the GFDL CM2.5 high-resolution coupled climate model. *J. Climate*, **25**, 2755–2781, doi:10.1175/JCLI-D-11-00316.1.

Emanuel, K. A., and D. Nolan, 2004: Tropical cyclone activity and the global climate system. *26th Conf. on Hurricanes and Tropical Meteorology*, Miami, FL, Amer. Meteor. Soc., 10A.2. [Available online at https://ams.confex.com/ams/26HURR/techprogram/paper_75463.htm.]

Giannini, A., M. A. Cane, and Y. Kushnir, 2001: Interdecadal changes in the ENSO teleconnection to the Caribbean region and the North Atlantic Oscillation. *J. Climate*, **14**, 2867–2879, doi:10.1175/1520-0442(2001)014<2867:ICITET>2.0.CO;2.

Gill, A. E., 1980: Some simple solutions for heat-induced tropical circulation. *Quart. J. Roy. Meteor. Soc.*, **106**, 447–462, doi:10.1002/qj.49710644905.

Gloersen, P., 1995: Modulation of hemispheric sea-ice cover by ENSO events. *Nature*, **373**, 503–506, doi:10.1038/373503a0.

Goldenberg, S. B., and L. J. Shapiro, 1996: Physical mechanisms for the association of El Niño and West African rainfall with Atlantic major hurricane activity. *J. Climate*, **9**, 1169–1187, doi:10.1175/1520-0442(1996)009<1169:PMFTAO>2.0.CO;2.

Jia, L., and Coauthors, 2015: Improved seasonal prediction of temperature and precipitation over land in a high-resolution GFDL climate model. *J. Climate*, **28**, 2044–2062, doi:10.1175/JCLI-D-14-00112.1.

Kalnay, E., and Coauthors, 1996: The NCEP/NCAR 40-Year Reanalysis Project. *Bull. Amer. Meteor. Soc.*, **77**, 437–471, doi:10.1175/1520-0477(1996)077<0437:TNYRP>2.0.CO;2.

Kennedy, J. J., N. A. Rayner, R. O. Smith, D. E. Parker, and M. Saunby, 2011: Reassessing biases and other uncertainties in sea surface temperature observations measured in situ since 1850: 2. Biases and homogenization. *J. Geophys. Res.*, **116**, D14104, doi:10.1029/2010JD015220.

Kirtman, B. P., and Coauthors, 2014: The North American multimodel ensemble: Phase-1 seasonal-to-interannual prediction; phase-2 toward developing intraseasonal prediction. *Bull. Amer. Meteor. Soc.*, **95**, 585–601, doi:10.1175/BAMS-D-12-00050.1.

Knapp, K. R., M. C. Kruk, D. H. Levinson, H. J. Diamond, and C. J. Neumann, 2010: The International Best Track Archive for Climate Stewardship (IBTrACS). *Bull. Amer. Meteor. Soc.*, **91**, 363–376, doi:10.1175/2009BAMS2755.1.

Kobayashi, S., and Coauthors, 2015: The JRA-55 Reanalysis: General specifications and basic characteristics. *J. Meteor. Soc. Japan*, **93**, 5–48.

Krishnamurthy, L., G. A. Vecchi, R. Msadek, H. Murakami, A. Wittenberg, and F. Zeng, 2016: Impact of strong ENSO on regional tropical cyclone activity in a high-resolution climate model in the North Pacific and North Atlantic Oceans. *J. Climate*, **29**, 2375–2394, doi:10.1175/JCLI-D-15-0468.1.

Kubota, H., and B. Wang, 2009: How much do tropical cyclones affect seasonal and interannual rainfall variability over the western North Pacific? *J. Climate*, **22**, 5495–5510, doi:10.1175/2009JCLI2646.1.

Lander, M. A., 1994: An exploratory analysis of the relationship between tropical storm formation in the western North Pacific and ENSO. *Mon. Wea. Rev.*, **122**, 636–651, doi:10.1175/1520-0493(1994)122<0636:AEAOTR>2.0.CO;2.

Lau, N.-C., and M. J. Nath, 2000: Impact of ENSO on the variability of the Asian–Australian monsoons as simulated in GCM experiments. *J. Climate*, **13**, 4287–4309, doi:10.1175/1520-0442(2000)013<4287:IOEOTV>2.0.CO;2.

Marler, T. E., 2014: Pacific island tropical cyclones are more frequent and globally relevant, yet less studied. *Front. Environ. Sci.*, **2**, 42, doi:10.3389/fenvs.2014.00042.

Matsuno, T., 1966: Quasi-geostrophic motions in the equatorial area. *J. Meteor. Soc. Japan*, **44**, 25–43.

Msadek, R., and Coauthors, 2014: Predicting a decadal shift in North Atlantic climate variability using the GFDL forecast system. *J. Climate*, **27**, 6472–6496, doi:10.1175/JCLI-D-13-00476.1.

Murakami, H., B. Wang, T. Li, and A. Kitoh, 2013: Projected increase in tropical cyclones near Hawaii. *Nat. Climate Change*, **3**, 749–754, doi:10.1038/nclimate1890.

——, G. A. Vecchi, T. L. Delworth, K. Paffendorf, R. Gudgel, L. Jia, and F. Zeng, 2015a: Investigating the influence of anthropogenic forcing and natural variability on the 2014 Hawaiian hurricane season [in "Explaining Extreme Events of 2014 from a Climate Perspective"]. *Bull. Amer. Meteor. Soc.*, **96** (12), S115–S119, doi:10.1175/BAMS-D-15-00119.1.

——, and Coauthors, 2015b: Simulation and prediction of category 4 and 5 hurricanes in the high-resolution GFDL HiFLOR coupled climate model. *J. Climate*, **28**, 9058–9079, doi:10.1175/JCLI-D-15-0216.1.

Philander, S. G. H., 1983: El Niño Southern Oscillation phenomena. *Nature*, **302**, 295–301, doi:10.1038/302295a0.

Pielke, R., Jr., and C. Landsea, 1999: La Niña, El Niño, and Atlantic hurricane damage in the United States. *Bull. Amer. Meteor. Soc.*, **80**, 2027–2033, doi:10.1175/1520-0477(1999)080<2027:LNAENO>2.0.CO;2.

——, J. Gratz, C. Landsea, D. Collins, M. Saunders, and R. Musulin, 2008: Normalized hurricane damage in the United States: 1900–2005. *Nat. Hazards Rev.*, **9**, 29–42, doi:10.1061/(ASCE)1527-6988(2008)9:1(29).

Rappaport, E. N., 2000: Loss of life in the United States associated with recent Atlantic tropical cyclones. *Bull. Amer. Meteor. Soc.*, **81**, 2065–2073, doi:10.1175/1520-0477(2000)081<2065:LOLITU>2.3.CO;2.

Rasmusson, E. M., and J. M. Wallace, 1983: Meteorological aspects of the El Niño/Southern Oscillation. *Science*, **222**, 1195–1202, doi:10.1126/science.222.4629.1195.

Rayner, N., D. Parker, E. Horton, C. Folland, L. Alexander, D. Rowell, E. Kent, and A. Kaplan, 2003: Global analyses of sea surface temperature, sea ice, and night marine air temperature since the late nineteenth century. *J. Geophys. Res.*, **108**, 4407, doi:10.1029/2002JD002670.

Revell, C. G., and S. W. Goulter, 1986: South Pacific tropical cyclones and the Southern Oscillation. *Mon. Wea. Rev.*, **114**, 1138–1145, doi:10.1175/1520-0493(1986)114<1138:SPTCAT>2.0.CO;2.

Rodgers, E. B., R. F. Adler, and H. F. Pierce, 2000: Contribution of tropical cyclones to the North Pacific climatological rainfall as observed from satellites. *J. Appl. Meteor.*, **39**, 1658–1678, doi:10.1175/1520-0450(2000)039<1658:COTCTT>2.0.CO;2.

Ropelewski, C. F., and M. S. Halpert, 1986: North American precipitation and temperature patterns associated with the El Niño/Southern Oscillation (ENSO). *Mon. Wea. Rev.*, **114**, 2352–2362, doi:10.1175/1520-0493(1986)114<2352:NAPATP>2.0.CO;2.

Straus, D. M., and J. Shukla, 2002: Does ENSO force the PNA? *J. Climate*, **15**, 2340–2358, doi:10.1175/1520-0442(2002)015<2340:DEFTP>2.0.CO;2.

Tartaglione, C. A., S. R. Smith, and J. J. O'Brien, 2003: ENSO impact on hurricane landfall probabilities for the Caribbean. *J. Climate*, **16**, 2925–2931, doi:10.1175/1520-0442(2003)016<2925:EIOHLP>2.0.CO;2.

Vecchi, G. A., and Coauthors, 2013: Multiyear predictions of North Atlantic hurricane frequency: Promise and limitations. *J. Climate*, **26**, 5337–5357, doi:10.1175/JCLI-D-12-00464.1.

——, and Coauthors, 2014: On the seasonal forecasting of regional tropical cyclone activity. *J. Climate*, **27**, 7994–8016, doi:10.1175/JCLI-D-14-00158.1.

Vitart, F., and T. N. Stockdale, 2001: Seasonal forecasting of tropical storms using coupled GCM integrations. *Mon. Wea. Rev.*, **129**, 2521–2537, doi:10.1175/1520-0493(2001)129<2521:SFOTSU>2.0.CO;2.

Wang, B., and J. C. L. Chan, 2002: How strong ENSO events affect tropical storm activity over the western North Pacific. *J. Climate*, **15**, 1643–1658, doi:10.1175/1520-0442(2002)015<1643:HSEEAT>2.0.CO;2.

——, and Q. Zhang, 2002: Pacific–East Asian teleconnection. Part II: How the Philippine Sea anomalous anticyclone is established during El Niño development. *J. Climate*, **15**, 3252–3265, doi:10.1175/1520-0442(2002)015<3252:PEATPI>2.0.CO;2.

Wu, G., and N.-C. Lau, 1992: A GCM simulation of the relationship between tropical-storm formation and ENSO. *Mon. Wea. Rev.*, **120**, 958–977, doi:10.1175/1520-0493(1992)120<0958:AGSOTR>2.0.CO;2.

Yang, X., and Coauthors, 2013: A predictable AMO-like pattern in the GFDL fully coupled ensemble initialization and decadal forecasting system. *J. Climate*, **26**, 650–661, doi:10.1175/JCLI-D-12-00231.1.

——, and Coauthors, 2015: Seasonal predictability of extratropical storm tracks in GFDL's high-resolution climate prediction model. *J. Climate*, **28**, 3592–3611, doi:10.1175/JCLI-D-14-00517.1.

Zebiak, S. E., and M. A. Cane, 1987: A model El Niño–Southern Oscillation. *Mon. Wea. Rev.*, **115**, 2262–2278, doi:10.1175/1520-0493(1987)115<2262:AMENO>2.0.CO;2.

Zhang, Q., Q. Liu, and L. Wu, 2009: Tropical cyclone damage in China: 1983–2006. *Bull. Amer. Meteor. Soc.*, **90**, 489–495, doi:10.1175/2008BAMS2631.1.

Zhang, S., and A. Rosati, 2010: An inflated ensemble filter for ocean data assimilation with a biased coupled GCM. *Mon. Wea. Rev.*, **138**, 3905–3931, doi:10.1175/2010MWR3326.1.

——, M. J. Harrison, A. Rosati, and A. Wittenberg, 2007: System design and evaluation of coupled ensemble data assimilation for global oceanic climate studies. *Mon. Wea. Rev.*, **135**, 3541–3564, doi:10.1175/MWR3466.1.

Zhang, W., H. F. Graf, Y. Leung, and M. Herzog, 2012: Different El Niño types and tropical cyclone landfall in East Asia. *J. Climate*, **25**, 6510–6523, doi:10.1175/JCLI-D-11-00488.1.

——, Y. Leung, and K. Fraedrich, 2015: Different El Niño types and intense typhoons in the western North Pacific. *Climate Dyn.*, **44**, 2965–2977, doi:10.1007/s00382-014-2446-4.

——, G. A. Vecchi, H. Murakami, G. Villarini, and L. Jia, 2016a: The Pacific meridional mode and the occurrence of tropical cyclones in the western North Pacific. *J. Climate*, **29**, 381–398, doi:10.1175/JCLI-D-15-0282.1.

——, and Coauthors, 2016b: Improved simulation of tropical cyclone responses to ENSO in the western North Pacific in the high-resolution GFDL HiFLOR coupled climate model. *J. Climate*, **29**, 1391–1415, doi:10.1175/JCLI-D-15-0475.1.

——, G. Villarini, G. A. Vecchi, H. Murakami, and R. Gudgel, 2016c: Statistical-dynamical seasonal forecast of western North Pacific and East Asia landfalling tropical cyclones using the high-resolution GFDL FLOR coupled model. *J. Adv. Model. Earth Syst.*, **8**, 538–565, doi:10.1002/2015MS000607.

——, G. A. Vecchi, G. Villarini, H. Murakami, A. Rosati, X. Yang, L. Jia, and F. Zeng, 2016d: Modulation of western North Pacific tropical cyclone activity by the Atlantic meridional mode. *Climate Dyn.*, doi:10.1007/s00382-016-3099-2, in press.

Zhang, Y., and I. M. Held, 1999: A linear stochastic model of a GCM's midlatitude storm tracks. *J. Atmos. Sci.*, **56**, 3416–3435, doi:10.1175/1520-0469(1999056<);3416:ALSMOA>2.0.CO;2.